Available online at www.sciencedirect.com
ScienceDirect
Global and Planetary Change 56 (2007) 387–398
GLOBAL AND PLANETARY CHANGE
www.elsevier.com/locate/gloplacha

Cyclone activity associated with the interannual seesaw oscillation of summer precipitation over northern Eurasia

Yoshiki Fukutomi [a,*], Kooiti Masuda [a], Tetsuzo Yasunari [a,b]

[a] *Frontier Research Center for Global Change, JAMSTEC, Yokohama, Japan*
[b] *Hydrospheric Atmsopheric Research Center, Nagoya University, Nagoya, Japan*

Received 25 April 2005; accepted 19 July 2006
Available online 24 October 2006

Abstract

This study describes surface cyclone activity associated with the interannual variability in summer precipitation in northern Eurasia and how that activity may be connected to other climate signals. An east–west seesaw oscillation of precipitation across Siberia is the primary mode of interannual variability in the summer hydrological cycle over northern Eurasia. This variation occurs at sub-decadal timescales of about 6–8 years. The spatial characteristics of cyclone frequency and cyclone tracks at the two poles in variability [eastern Siberia (ES)-wet–western Siberia (WS)-dry and WS-wet–ES-dry] were examined, and temporal variability in regional cyclone frequency was compared to basin-scale precipitation variability. The analysis period was from 1973 to 2002, when the precipitation variability signal was predominant.

Cyclone behavior suggested that the regions of enhanced (reduced) cyclone activity coincided with regions of increased (decreased) precipitation in each phase of the oscillation. Such behavior reflects the zonal displacement of the track of frequent storm activity that accompanies the changes in precipitation. Comparisons of the temporal characteristics confirmed the importance of regional cyclone frequency on precipitation variability in both eastern and western Siberia. Low-frequency changes in regional cyclone activity may produce the precipitation oscillation. We used various climate signals to explore connections between regional precipitation and cyclone activity in Siberia. Results suggest that the North Atlantic Oscillation (NAO) from the preceding winter is significantly and negatively correlated with summer surface cyclone frequency and precipitation over western Siberia. Enhanced (reduced) summer cyclone activity and precipitation in western Siberia follows low- (high-) winter NAO. However, the physical mechanisms linking summer cyclone activity and precipitation over western Siberia with the preceding climate conditions associated with the winter NAO remain unclear.

Keywords: cyclone activity; interannual variability of summer precipitation; Siberia; North Atlantic Oscillation

1. Introduction

An east–west precipitation oscillation is a noteworthy characteristic of the interannual variability in the summer (June–August: JJA) hydrological cycle over northern Eurasia (Fukutomi et al., 2003, 2004). An out-of-phase relationship exists in the spatial and temporal variation in large-river-basin-scale summer precipitation

* Corresponding author. Frontier Research Center for Global Change, Yokohama Institute for Earth Sciences, Japan Agency for Marine-Earth Science and Technology (JAMSTEC), 3173-25 Showamachi, Kanazawa-ku, Yokohama, Kanagawa 236-0001, Japan. Tel.: +81 45 778 5539; fax: +81 45 778 5706.
E-mail address: fukutomi@jamstec.go.jp (Y. Fukutomi).

0921-8181/$ - see front matter © 2006 Elsevier B.V. All rights reserved.
doi:10.1016/j.gloplacha.2006.07.026

between eastern and western Siberia (hereafter ES and WS). The spatial precipitation anomaly acquires an east–west dipole pattern at the extreme poles of the oscillation. The variation shows sub-decadal timescales of about 6–8 years and has been especially pronounced since the early 1970s. This oscillation is referred to as a precipitation seesaw. Large-scale circulation anomalies during the extreme phases show a quasi-stationary wave pattern across northern Eurasia.

Fukutomi et al. (2004) showed that interannual changes in storm-track activity aligned with the Arctic frontal zone over northern Eurasia play a dynamic role in maintaining the mean circulation pattern at the extreme ends of the oscillation. They used variance statistics for synoptic-scale (<10 days) eddy components to highlight the zonal displacement of high storm activity. Such displacement is reflected in geographical changes in the primary paths of traveling synoptic-scale weather systems. The dynamic effects of synoptic processes were diagnosed in terms of transient eddy statistics (Fukutomi et al., 2004), but the actual behavior of continental cyclones associated with the precipitation oscillation remains unclear.

Interannual increases (decreases) in annual discharge from major Siberian rivers are controlled by enhanced (reduced) activity of high-latitude summer cyclones and their attendant precipitation (Semiletov et al., 2000). Summer cyclone activity controls the strength of the hydrological cycle. Serreze and Etringer (2003) recently established a seasonal climatology that relates daily precipitation events in Siberian river basins with synoptic circulation types. They classified 500-hPa troughs (cyclonic flow) associated with heavy precipitation events in the river basins and revealed that both 500-hPa trough features and surface cyclogenesis counts are good proxies for day-to-day precipitation events (storminess) in individual basins. These previous studies have suggested that large-scale changes in the frequency of cyclones help to control basin-scale precipitation variability. Therefore, it is reasonable to expect that northern Eurasian cyclone activity is a major influence on the precipitation oscillation and the associated hydroclimate. However, little work has elucidated the substantial interannual relationships between basin-scale precipitation and cyclone activity that occurs over northern Eurasia in summer. It is necessary to investigate the statistical features of cyclones as main precipitating systems to understand the underlying mechanisms influencing long-term changes in the summer hydrological cycle over Siberia.

This study extends previous work (Fukutomi et al., 2004) to storm statistics using a Lagrangian-type approach. We sought to identify where extratropical cyclones that are associated with the precipitation oscillation form and move, and to confirm that interannual changes in large-scale cyclone activity play an important forcing role in the precipitation oscillation. Spatial characteristics of cyclone frequency and tracks that are characteristic of the two opposite extremes of the precipitation oscillation (ES-wet–WS-dry and WS-wet–ES-dry) were examined. Temporal variations in regional cyclone frequency were then compared to changes in basin-scale precipitation. The analysis period was 1973–2002, when the precipitation seesaw signal was predominant. This paper describes results that support evidence from previous work and discusses possible links to other climate factors.

2. Data

We used storm-track statistics for the Northern Hemisphere (NH) obtained from the National Oceanic and Atmospheric Administration (NOAA)/Climate Diagnostics Center (CDC). The surface cyclone statistics were derived from sea level pressure (SLP) data from the National Centers for Environmental Prediction (NCEP)–National Center for Atmospheric Research (NCAR) reanalysis. Detection of and tracking of surface cyclones in this dataset followed an algorithm originally developed by Serreze (1995) and Serreze et al. (1997). Cyclone statistics were consistent with those used in other studies (e.g., Clark et al., 1999; Serreze et al., 2001; McCabe et al., 2001; Serreze and Etringer, 2003). The cyclone detection algorithm was applied to 6-hourly SLP fields interpolated from a 2.5°×2.5° latitude–longitude grid to a 250-km version of the NH EASE-grid (Armstrong and Brodzik, 1995). The statistics for this study were for the period 1948 to present.

A Global Cyclone Climatology derived from the NCEP–NCAR reanalysis geopotential height fields between 1957 and 1998 (Key and Chan, 1999) was also used. This dataset was provided by the Cooperative Institute for Meteorological Satellite Studies (CIMSS) at the University of Wisconsin; it includes 12-hourly positions of cyclone centers and cyclone tracks at the 1000-hPa and 500-hPa levels at a grid resolution of 2.5°×5° latitude–longitude. In this analysis, 500-hPa cyclone centers and tracks for individual years in NH summer were extracted from the original record. Konard (2001) used the 500-hPa cyclone statistics from this dataset to investigate relationships between mid-tropospheric cyclones and extreme precipitation events.

As in previous studies, monthly global land precipitation analyses [PREC/L (Chen et al., 2002)] captured the spatial and temporal patterns of interannual summer

precipitation variability in Siberia. The precipitation data were on a 2.5° latitude–longitude grid. Data were available from 1948 to the present at the NOAA/Climate Prediction Center (CPC).

North Atlantic Oscillation (NAO) index data were from http://www.cgd.ucar.edu/~jhurrell/nao.html. These NAO indices were calculated as the difference in normalized sea level pressure between Ponta Delgada in the Azores and Reykjavik, Iceland. This definition of the NAO index differs from that used by Hurrell (1996). NAO data were used to determine the relationship between regional cyclone occurrences and the NAO. Note Hurrell (2003) describes basic characteristics of the NAO.

3. Results

3.1. Siberian precipitation seesaw

An interannual oscillation in precipitation occurs over Siberia that assumes a seesaw pattern. This section emphasizes that the precipitation seesaw is the leading interannual pattern of summer precipitation variability over northern Eurasia, as noted in earlier work (Fukutomi et al., 2003, 2004).

ES and WS precipitation indices, as well as a unified index that combines them, were derived to identify seesaw extremes used to construct composites of precipitation, cyclone frequency, and cyclone tracks. Fig. 1a

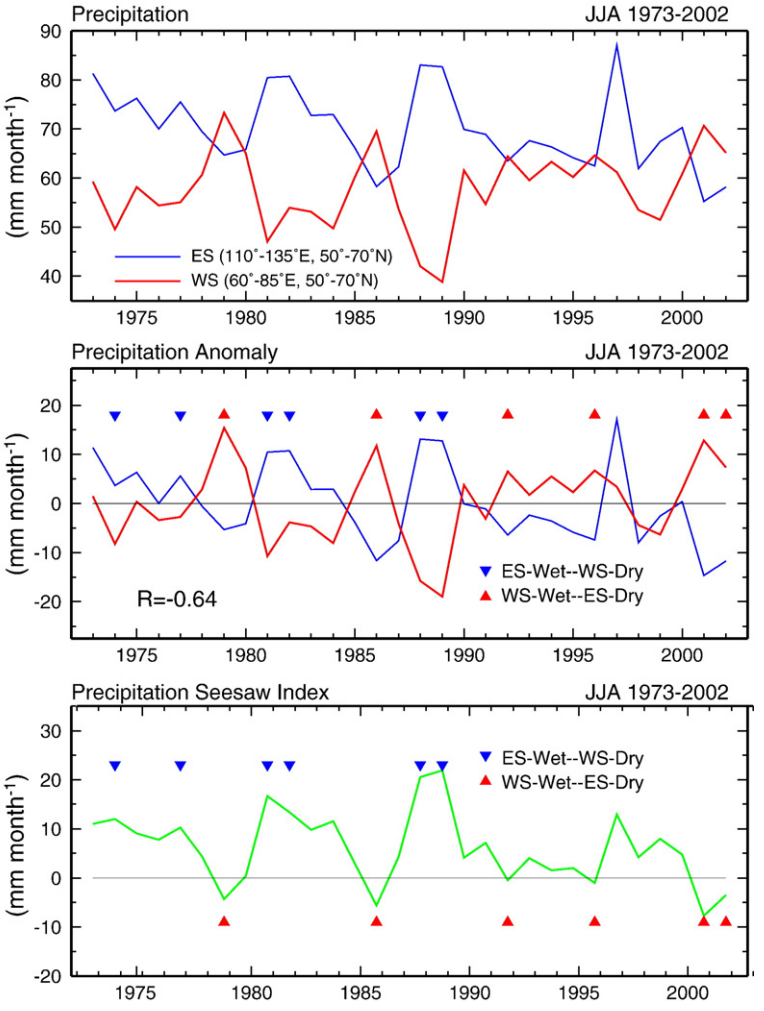

Fig. 1. (a) Time series of summer (JJA) mean precipitation (mm month^{-1}) for the ES domain (blue thin line: 110°–135°E, 50°–75°N) and the WS domain (red thick line: 60°–85°E, 50°–75°N). (b) Same as (a) except for anomalies. Six ES-wet–WS-dry summers (blue inverted triangles) and six WS-wet–ES-dry summers (red triangles) are selected. (c) Precipitation seesaw index (see text). The selected six ES-wet–WS-dry summers (six WS-wet–ES-dry summers) are indicated by blue inverted triangles (red triangles).

shows time series of average summer precipitation indices for ES and WS for 1973–2003. The precipitation index for ES (P_{ES}) is defined as the spatial average of JJA mean precipitation over the ES region (110°–135°E, 50°–70°N). The precipitation index for WS (P_{WS}) is similarly defined for (60°–85°E, 50°–70°N). These regions were defined following Serreze et al. (2003) and covered roughly the Lena (ES) and Ob (WS) River basins. Fig. 1b shows time series of index anomaly, which was computed as a deviation from the 30-yr climatology. The precipitation seesaw index (hereafter PSI) was defined as half the difference between them: $((P_{ES}-P_{WS})/2$;

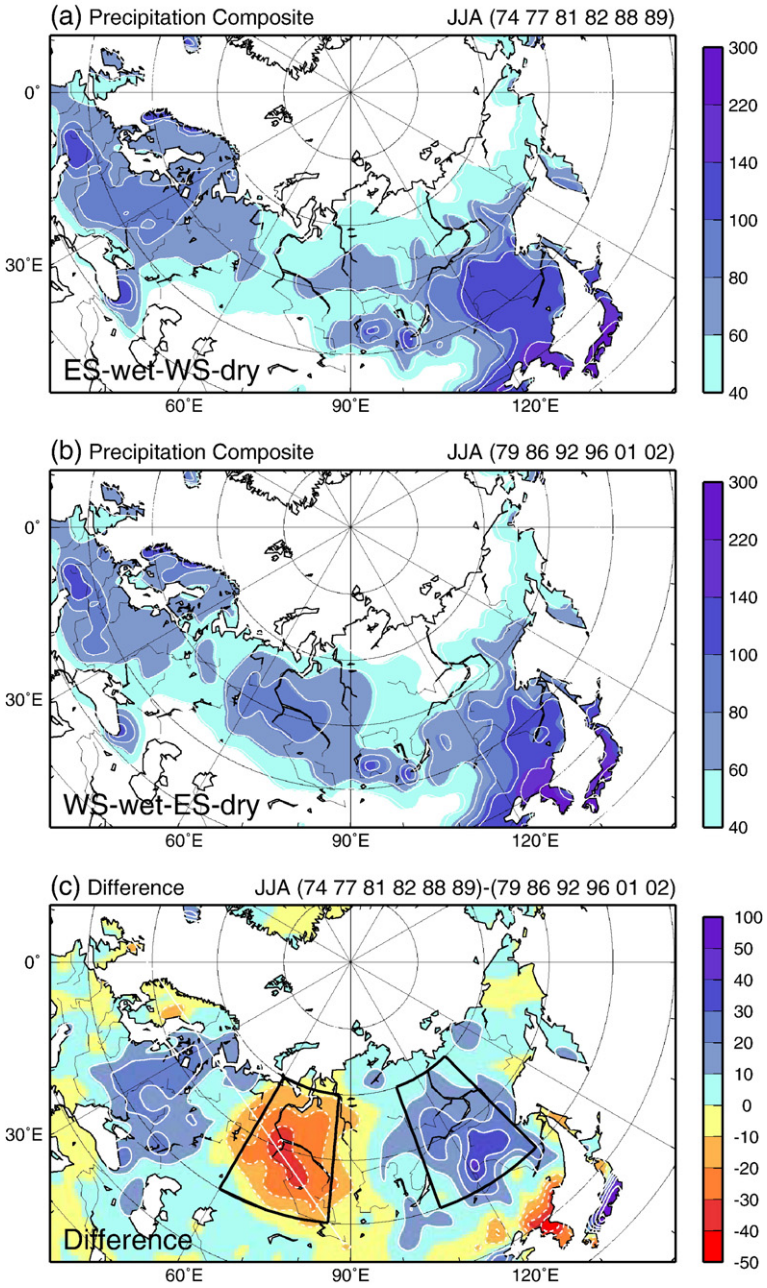

Fig. 2. (a) Composite of the summer mean precipitation (mm month^{-1}) defined for the six ES-wet–WS-dry summers. (b) Same as (a) except for the six WS-wet–ES-dry summers. (c) Composite difference between the two phases. The ES and WS regions that are used to define the precipitation indices are indicated by black boxes. Positive (negative) values are indicated by solid (dashed) lines.

Fig. 1c). Positive extremes of PSI represent ES-wet–WS-dry summers, and negative extremes of PSI represent WS-wet–ES-dry summers.

The two opposite poles of the seesaw were detected using P_{ES}, P_{WS}, and PSI. The extremes were the six highest ES-wet–WS-dry summers (1974, 1977, 1981, 1982, 1988, and 1989) and the six highest WS-wet–ES-dry summers (1979, 1986, 1992, 1996, 2001, and 2002). When the ES region was very wet (above-normal precipitation), the WS region was very dry (below-normal precipitation), and vice versa. The following conditions were considered in choosing the extremes: 1) ES-wet–WS-dry (WS-wet–ES-dry) summers are the highest (lowest) phases of the PSI (Fig. 1c). 2) Pairs

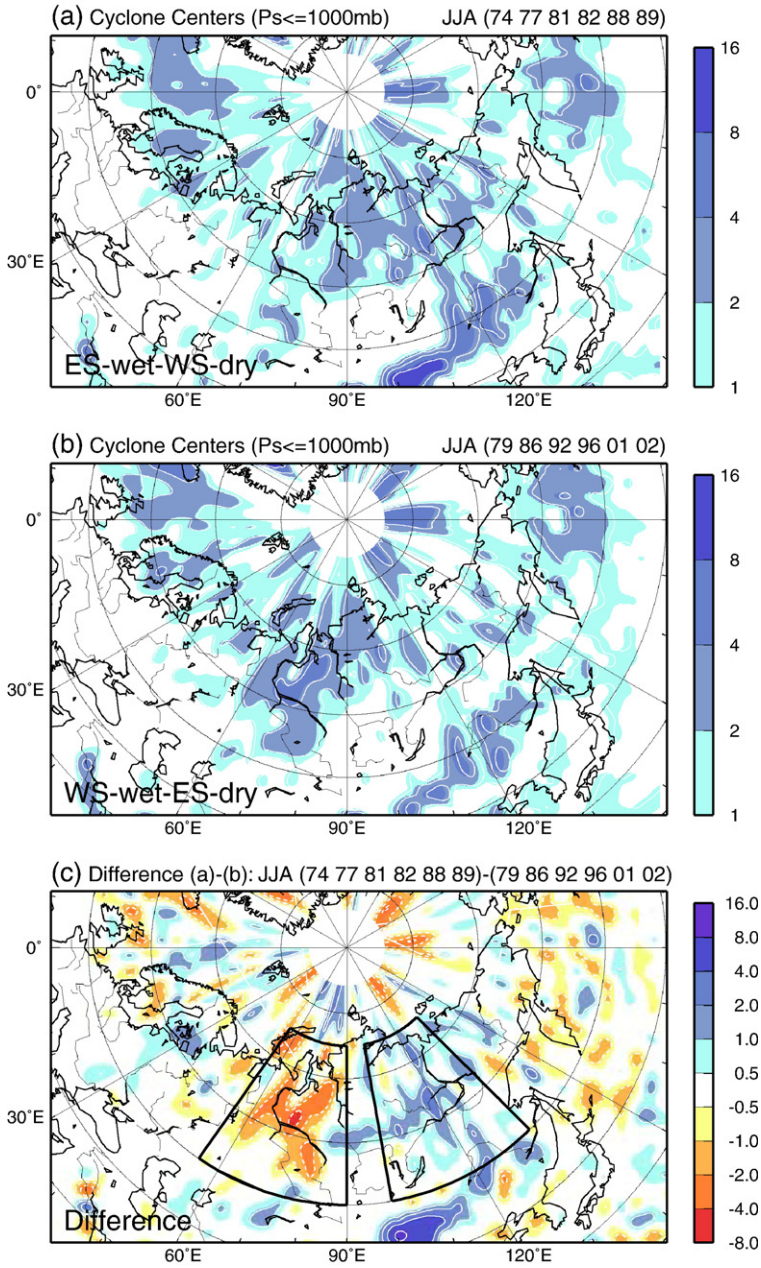

Fig. 3. (a) Composite of cyclone frequency (cyclone/250×250 km^2/season) for the six ES-wet–WS-dry summers. (b) Same as (a) except for the six WS-wet–ES-dry summers. (c) Composite difference between the two phases. Positive (negative) values are indicated by solid (dashed) lines. Boxes E (100°–135°E, 50°–75°N) and W (55°–90°E, 50°–75°N) are outlined by heavy black lines (see text). Artifacts in the area 85°–90°N are masked out.

of positive P_{ES} and negative P_{WS} anomalies for the ES-wet–WS-dry summers (positive P_{WS} and negative P_{ES} anomalies for the WS-wet–ES-dry summers) (Fig. 1b). Composites were constructed based on these criteria.

The Siberian precipitation seesaw follows a characteristic pattern. Fig. 1a and b shows that the two precipitation indices give rise to a clear out-of-phase behavior, as noted by Fukutomi et al. (2003, 2004). We found a significant negative correlation ($r=-0.64$) between these two indices that exceeds the 99.9% confidence level ($r=-0.57$) according to a standard *t*-test assuming 28 degrees of freedom. The precipitation composite for ES-wet–WS-dry summers shows a striking increase in central-ES and a decrease in WS (Fig. 2a). In contrast, the composite for the WS-wet–ES-dry summers shows more precipitation over WS than ES (Fig. 2b). The precipitation anomaly pattern, defined as the difference between the two composite precipitation fields (Fig. 2c), shows a clear east–west dipole pattern across Siberia. Additionally, one can notice that another center of comparatively weaker anomalies is located over Eastern Europe. The relationship between this upstream signal and the Siberian dipole pattern is worth investigating, however, that is not our present concern. The whole pattern is basically similar to that presented by Fukutomi et al. (2004, Fig. 3d).

3.2. Large-scale changes in cyclone activity associated with the precipitation seesaw

The frequency of surface cyclones over Siberia as a function of the phase of the precipitation seesaw was examined using the CDC storm-track data. Composites of cyclone frequency (Fig. 3) were constructed with methods

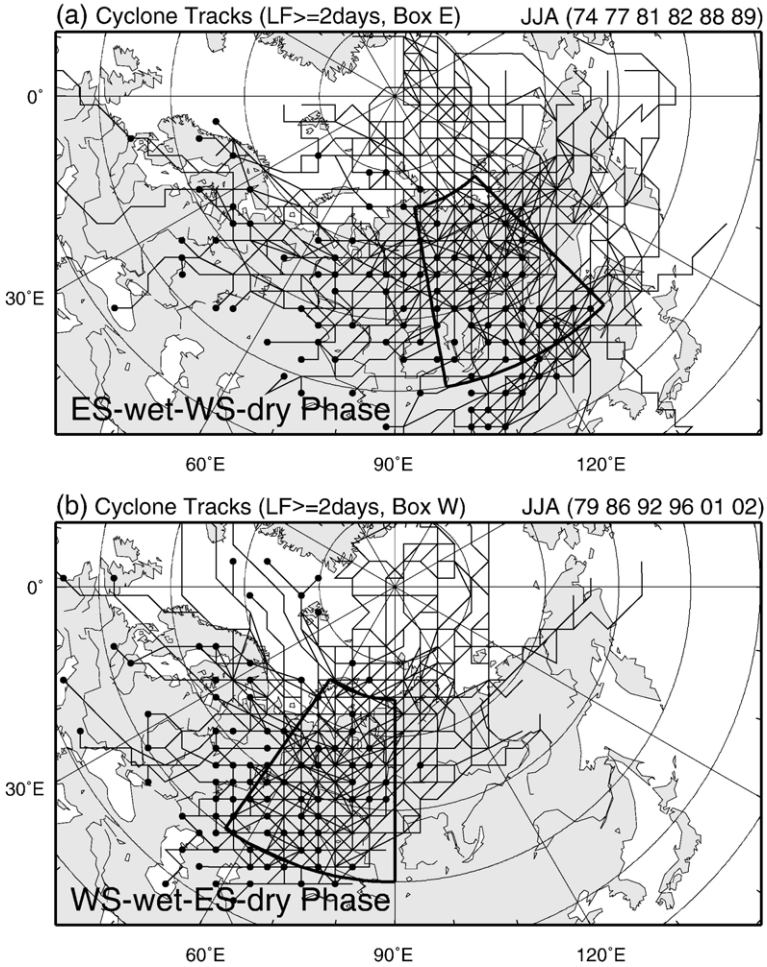

Fig. 4. (a) Cyclone tracks passing through box E and their genesis points (dots) for the six ES-wet–WS-dry summers. (b) Same as (a) except for box W for the six WS-wet–ES-dry summers.

used for Fig. 2. Cyclone frequency was defined as the number of cyclone centers per summer at each EASE grid point. Weak systems were ignored; only cyclones with central pressures at or below 1000 hPa were included. This central pressure cut-off reduced the number of non-precipitating weather systems in the total counts. Accordingly, the resulting statistics reflect precipitation-bearing cyclone activity.

Fig. 3a shows the geographical distribution of cyclone frequency for the ES-wet–WS-dry summers. There were several local maxima in central-ES (east of 90°E). These maxima corresponded closely to regions

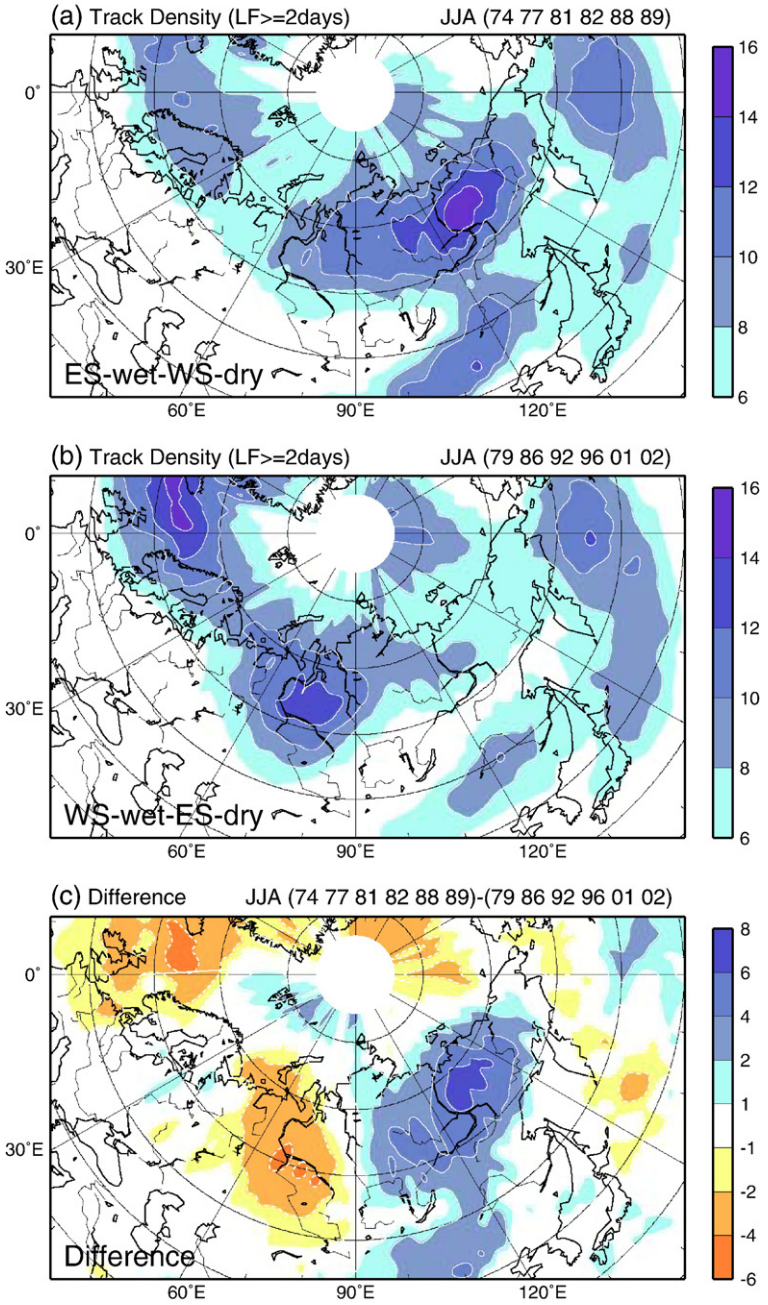

Fig. 5. (a) Composite of cyclone track density (tracks/555 km circle/season) for the six ES-wet–WS-dry summers. (b) Same as (a) except for the six WS-wet–ES-dry summers. (c) Composite difference between the two phases. Positive (negative) values are indicated by solid (dashed) lines. Artifacts in the area 85°–90°N are masked out.

of increased precipitation in central and eastern Siberia (Fig. 2a). In contrast, a pronounced maximum prevailed over much of WS during WS-wet–ES-dry summers (Fig. 3b), a frequency maximum that overlapped a band of heavier precipitation across WS (Fig. 2b). In summary, cyclone occurrence increased (decreased) close to or within regions of above- (below-) normal precipitation. Locations of relatively high cyclone frequency matched those in a climatology obtained by Chen et al. (1991) and Chen and Zhang (1996). Composite difference fields between the two contrasting extremes (ES-wet–WS-dry summers minus WS-wet–ES-dry summers; Fig. 3c) show a dipole pattern very similar to that of precipitation (Fig. 2c).

Fig. 3c includes two domains outlined by heavy solid lines, which characterize the spatial behavior of cyclone tracks and temporal variation in regional cyclone frequency. One domain roughly covers ES and is defined as box E (100°–135°E, 50°–75°N); a second domain covers WS and is defined as box W (55°–90°E, 50°–75°N). These domains encompass the regions of high and low cyclone activity associated with the precipitation seesaw.

Fig. 4 shows the distributions of surface cyclone tracks in each extreme phase to reveal preferred cyclone paths that affect regions of increased precipitation. Cyclone tracks with at least one central pressure at or below 1000 hPa and a minimum lifetime of 2 days were extracted from the CDC storm-track data. Weak and shorter-lived weather systems were ignored. Only cyclones that passed through, originated in, or terminated in box E (box W) were plotted for the ES-wet–WS-dry summers (WS-wet–ES-dry summers). Thus, cyclone tracks clustered in the targeted boxes. However, regions of significant cyclogenesis and cyclolysis were scattered over northern Eurasia. During the ES-wet–WS-dry summers (Fig. 4a), most of the cyclones passing over eastern Siberia developed inside Siberia. After crossing ES, the cyclones typically moved northeastward toward the Arctic Ocean and the Kolyma region. Some of them reached the North Pacific. Several cyclones developed in Northeast Europe and Scandinavia (west of 60°E), and a few entered from the Kara Sea. They subsequently moved eastward and southeastward to central–eastern Siberia. A considerable number of cyclones developed within and then exited ES; cyclogenesis was common in this region. During the WS-wet–ES-dry summers (Fig. 4b), cyclones entering western Siberia came from various locations: European, central Asia, and the Norwegian Sea. Many cyclones also developed inside western Siberia. This region is strongly cyclogenetic. Most cyclones moved eastward and northeastward, eventually reaching central and eastern Siberia and the Arctic Ocean.

A more comprehensive picture of geographical changes in primary cyclone tracks is provided in Fig. 5,

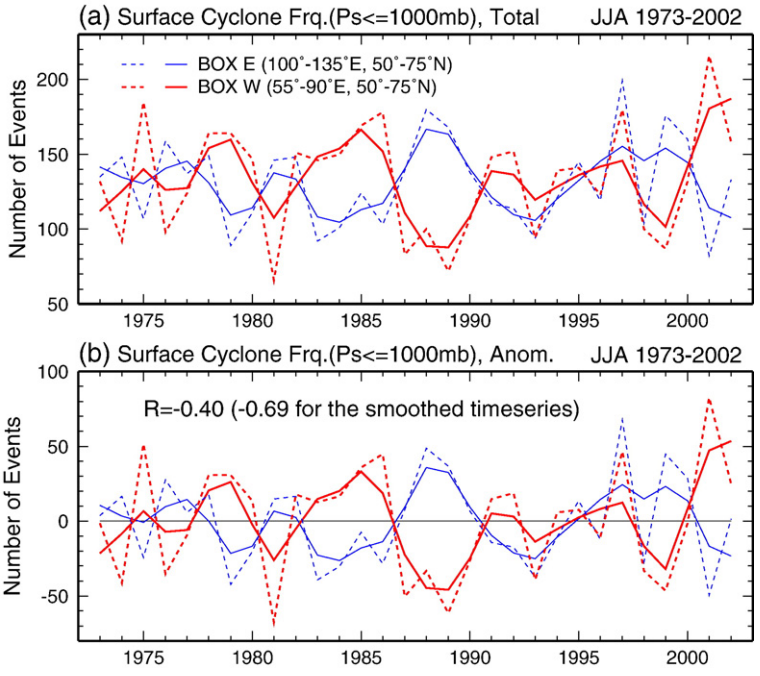

Fig. 6. (a) Time series of summer (JJA) cyclone counts for box E (blue) and box W (red). Dashed (solid) line is raw (smoothed) time series. (b) Same as (a) except for anomalies.

which shows composites of cyclone track density constructed for the opposite phases of the precipitation seesaw as in Fig. 3. Cyclone track density is the number of cyclones passing within a certain distance of each grid point and was computed as described by Sinclair (1994). Track density was derived by counting the tracks in overlapping circular cells with a radius of 555 km (approximately 5° latitude). This technique is spatially smoother compared to raw counts that are based on non-overlapping contiguous unit cells (e.g., Sinclair, 1994, 1995). The map for the ES-wet–WS-dry phase (Fig. 5a) shows a high density between 60°–70°N latitude extending from the eastern end of WS into Kolyma. The enhanced track density across central-ES was near the increased precipitation signal in ES (Fig. 2a,c). The cyclone frequency maxima in central and ES (Fig. 3a) fell within this band. At the same time, density was relatively low over WS. In the WS-wet–ES-dry phase (Fig. 5b), there was a pronounced maximum in the same latitude belt over WS, and this high concentration of cyclone tracks overlapped the enhanced cyclonic activity (Fig. 3b) and the increased precipitation over WS (Fig. 2b). In contrast, the density was reduced over central and ES. The composite difference between the two phases (Fig. 5c) shows an east–west dipole, which is almost collocated with the precipitation dipole (Fig. 2c).

Cyclone behavior indicates that regions of enhanced (reduced) cyclone activity nearly coincide with regions of increased (decreased) precipitation in each seesaw phase. Results shown here for cyclone frequency and cyclone tracks agree with the zonal displacement of high storm-track activity that accompanies the precipitation seesaw as discussed by Fukutomi et al. (2004).

3.3. Interannual variability of regional cyclone activity and precipitation

Composite analyses of cyclone occurrence showed that spatial variability in storm-track activity resulted in the east–west precipitation pattern in the seesaw extremes. Temporal variations in summer precipitation in ES and WS are strongly linked to variations in regional cyclone activity. To show this linkage, temporal variations in summer cyclone counts between ES and WS were compared. Cyclone centers were counted for all grid points within box E (ES) and box W (WS). Fig. 6 presents time series of cyclone counts (i.e., area total cyclone frequency) for the two boxes in each summer from 1973–2002. The series of total counts (Fig. 6a) and anomalies (Fig. 6b) both displayed considerable interannual variability. Time series were

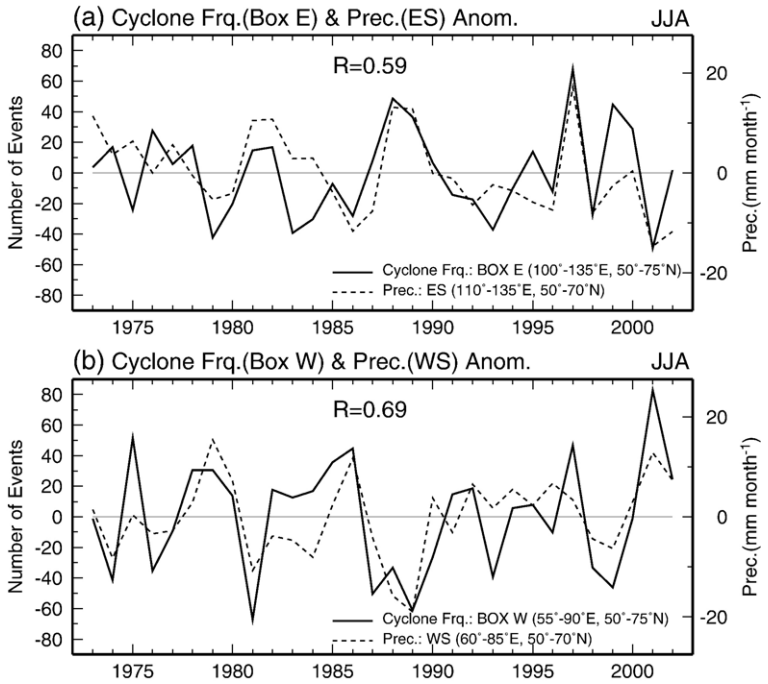

Fig. 7. (a) Time series of summer cyclone counts anomalies for box E (solid line) and summer precipitation anomalies averaged over the ES domain (dashed line). (b) Same as (a) except for box W (solid line) and the WS region (dashed line).

smoothed with a 3-point weighting average (1-2-1) to highlight lower-frequency interannual (sub-decadal) range signals. The two time series were out of phase. The correlation coefficient between raw counts for box E and box W was −0.40, which was significant at the 95% level. In addition, the correlation for the smoothed counts was −0.69. These inverse relationships reflect the seesaw nature of summer cyclone activity across Siberia.

Consider the relationship between summer precipitation and cyclone activity in each region during the same period (Fig. 7). A comparison of the time series of regional cyclone counts to those of precipitation anomalies revealed an apparent synchronous relationship for both the ES and WS region. Comparison of the two time series for ES (Fig. 7a) shows a variation in cyclone counts that is in phase with precipitation variability. The same is true over WS (Fig. 7b). Correlation coefficients between the two times series were 0.59 and 0.69 for ES and WS, respectively. Both were significant at a confidence level exceeding 99.9%. Interannual variability in cyclone frequency in box E (W) accounted for interannual variability in the area-averaged precipitation in the ES (WS) region.

4. Discussion

We examined the relationships between the seesaw pattern in summer precipitation and the concurrent cyclone activity over northern Eurasia. Statistics of cyclone frequency and cyclone tracks were used to measure cyclone behavior. Composite analyses presented a coherent picture of cyclone behavior affecting east–west patterns of precipitation in the seesaw extremes. Zonal displacement of cyclone activity played a key role in determining the seesaw pattern. Furthermore, results from comparisons of the temporal characteristics confirm the importance of regional cyclone frequency to the variability of precipitation in eastern and western Siberia. Consequently, the low-frequency changes in regional cyclone activity could result in the precipitation seesaw rhythm noted over the past 30 years.

Fukutomi et al. (2004) noted that the causes of interannual variability in cyclone (i.e., storm track) activity associated with the precipitation seesaw remain uncertain. Mechanisms responsible for year-to-year changes in large-scale baroclinicity over northern Eurasia and its link to other climate signals are not yet understood. To elucidate a relationship, the relationships

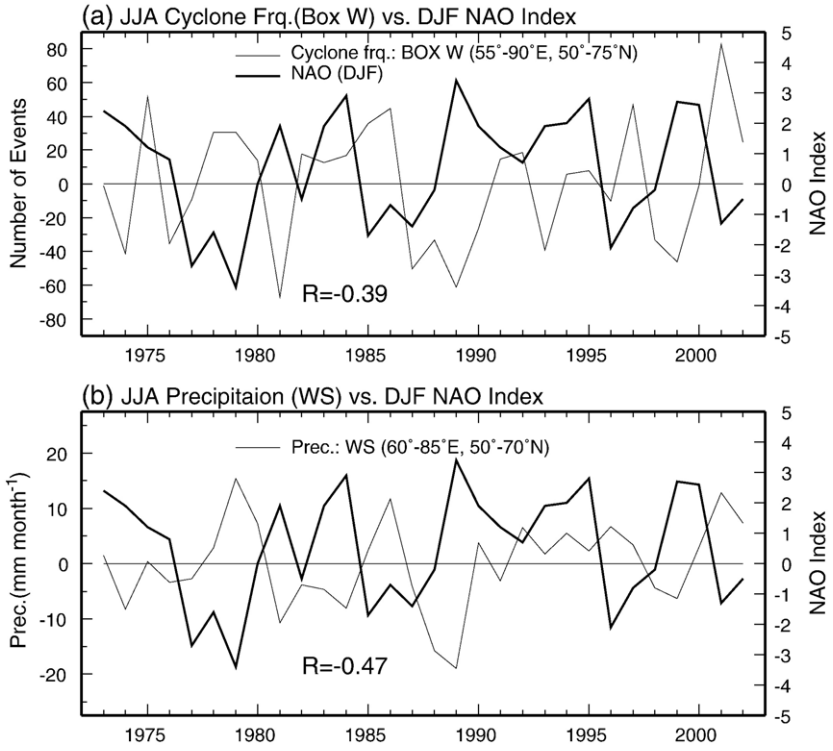

Fig. 8. (a) Time series of summer cyclone counts anomalies for box W (thin solid line) and the winter (DJF) NAO index (thick solid line). (b) Same as (a) except for summer precipitation anomalies (thin solid line) for the WS region.

between the Siberian regional cyclone activity, precipitation, and various climate indices were investigated (data not presented). No concurrent climate factors were found to produce the interannual signals. However, we did observe noteworthy two-season lagged relations. Panels a and b of Fig. 8 show that the preceding winter NAO is statistically related to the summer surface cyclone frequency and precipitation over WS. The correlation coefficient between the winter NAO and the summer cyclone frequency in box W was −0.39 for 1973–2002, which was marginally significant at the 95% confidence level. The correlation coefficient for precipitation had a higher value (−0.47) with the 99% confidence level. Summer cyclone frequency and precipitation in box E (ES) were poorly correlated with the winter NAO index. Similarly, the statistical relationships between WS regional 500-hPa cyclone frequency and the winter NAO index were examined using available data (not shown). The resulting correlation coefficient was −0.38 for 1958–1997 (−0.51 for 1968–1997), which marginally exceeded the 95 (99.5)% confidence level. These inverse relationships indicate that enhanced (reduced) summer cyclone activity and precipitation in WS followed low- (high-) winter NAO. However, mechanisms to explain these coherent signals are lacking. A question raised here is whether the climate conditions associated with the winter NAO influence subsequent summer storm activity in WS. Several recent studies have suggested potential impacts of the winter NAO and the following spring–summer surface climate signals over the Eurasian continent (e.g., Bojariu and Gimeno, 2003; Yu and Zhou, 2004; Wang and You, 2004). The winter NAO is a statistical predictor for subsequent summer climate over Eurasia; however, physical mechanisms underlying the delayed impact remain elusive.

A current concern is how the interannual background conditions influence summer cyclone activity and precipitation across northern Eurasia. What are the sources of variability? If the winter NAO changes summer storm activity as hypothesized from statistics, how is the climate memory transmitted to control summer storm activity? A plausible mechanism could be the seasonal progress of land-surface hydrological processes associated with continental snow mass and soil moisture provided by snowmelt water and feedback into the atmosphere (e.g., Barnett et al., 1989; Yasunari et al., 1991; Bamzai and Marx, 2000). However, soil moisture does not appear to be the bridge linking winter–spring snow cover and subsequent summer conditions over northern Eurasia (e.g., Shinoda, 2001; Robock et al., 2003). Puzzling issues remain for the role of a carrier of climate signals as discussed by Hori and Yasunari (2003). Further careful investigation with regard to the winter–spring snow cover, snow mass, and soil moisture is required to detect the primary driver of the dominant mode of summer hydroclimate variability in northern Eurasia.

Acknowledgments

The authors wish to thank two anonymous reviewers for their comments. We want also to thank Hiromichi Igarashi (FRCGC/JAMSTEC) for helpful discussions, and Nobuhiko Endo (FRCGC/JAMSTEC) for assistance to processing the cyclone climatology data. Storm-tracks dataset based on SLP is available online at the NOAA/CDC (ftp://ftp.cdc.noaa.gov/Datasets/map/storm/). Global Cyclone Climatology dataset based on geopotential height is provided at CIMSS, University of Wisconsin–Madison (ftp://stratus.ssec.wisc.edu/pub/cyclones/).

References

Armstrong, R.L., Brodzik, M.J., 1995. An earth-gridded SSM/I data set for cryospheric studies global change monitoring. Adv. Space Res. 16, 155–163.

Bamzai, A.S., Marx, L., 2000. COLA AGCM simulation of the effect of anomalous spring snow over Eurasia on the Indian summer monsoon. Q. J. R. Meteorol. Soc. 126, 2575–2584.

Barnett, T.P., Dumenil, L., Schlese, U., Roeckner, E., Latif, M., 1989. The effect of Eurasian snow cover on regional and global climate variations. J. Atmos. Sci. 46, 661–685.

Bojariu, R., Gimeno, L., 2003. The role of snow cover fluctuations in multiannual NAO persistence. Geophys. Res. Lett. 30, 1156, doi:10.1029/2002GL015651.

Chen, S.J., Zhang, P.Z., 1996. Climatology of deep cyclones over Asia and the Northwest Pacific. Theor. Appl. Climatol. 54, 139–146.

Chen, S.J., Kuo, Y.H., Zhang, P.Z., Bai, Q.F., 1991. Synoptic climatology of cyclogenesis over East Asia, 1958–1987. Mon. Weather Rev. 119, 1407–1418.

Chen, M., Xie, P., Janowiak, J.E., Arkin, P.A., 2002. Global land precipitation: a 50-yr monthly analysis based on gauge observations. J. Hydrometeorol. 3, 249–266.

Clark, M.P., Serreze, M.C., Robinson, D.A., 1999. Atmospheric controls on Eurasian snow extent. Int. J. Climatol. 19, 27–40.

Fukutomi, Y., Igarashi, H., Masuda, K., Yasunari, T., 2003. Interannual variability of summer water balance components in three major river Basins of northern Eurasia. J. Hydrometeorol. 4, 283–296.

Fukutomi, Y., Masuda, K., Yasunari, T., 2004. The role of storm track activity in the interannual seesaw of summer precipitation over northern Eurasia. J. Geophys. Res. 109 (D2), D02109, doi:10.1029/2003JD003912.

Hori, M.E., Yasunari, T., 2003. NAO impact towards the springtime snow disappearance in the western Eurasian continent. Geophys. Res. Lett. 30, 1977, doi:10.1029/2003GL018103.

Hurrell, J.W., 1996. Influence of variations in extratropical wintertime teleconnections on Northern Hemisphere temperature. Geophys. Res. Lett. 23, 665–668.

Hurrell, J.W., 2003. An overview of the North Atlantic Oscillation. In: Hurrell, J.W., Kushnir, Y., Ottersen, G., Visbeck, M. (Eds.), The North Atlantic Oscillation: Climate Significance and Environmental Impact. Geophysical Monograph, vol. 134. American Geophysical Union, Washington, DC, The USA, pp. 1–35.

Key, J.R., Chan, A.C.K., 1999. Multidecadal global and regional trends in 1000mb and 500mb cyclone frequencies. Geophys. Res. Lett. 26, 2053–2056.

Konard, C.E., 2001. The most extreme precipitation events over the eastern United States from 1950 to 1996: considerations of scale. J. Hydrometeorol. 2, 309–325.

McCabe, G.J., Clark, M.P., Serreze, M.C., 2001. Trends in Northern Hemisphere surface cyclone frequency and intensity. J. Climate 14, 2763–2768.

Robock, A., Mu, M., Vinnikov, K., Robinson, D., 2003. Land surface conditions over Eurasia and Indian summer monsoon rainfall. J. Geophys. Res. 108 (D4), 4131, doi:10.1029/2002JD002286.

Semiletov, I.P., Savelieva, N.I., Weller, G.E., Pipko, I.I., Pugach, S.P., Gukov, A.Yu., Vasilevskaya, L.N., 2000. The dispersion of Siberian river flows into coastal waters: meteorological, hydrological and hydrochemical aspects. In: Lewis, E.L., Jones, E.P., Lemke, P., Prowse, T.D., Wadhams, P. (Eds.), The Freshwater Budget of the Arctic Ocean. NATO Science Series 2: Environmental Security, vol. 47. Kluwer Academic Publishers, Dordrecht, The Netherlands, pp. 323–366.

Serreze, M.C., 1995. Climatological aspects of cyclone development and decay in the Arctic. Atmos.-Ocean 33, 1–23.

Serreze, M.C., Etringer, A.J., 2003. Precipitation characteristics of the Eurasian Arctic drainage system. Int. J. Climatol. 23, 1267–1291.

Serreze, M.C., Rogers, J.C., Carse, F., Barry, R.G., 1997. Icelandic low cyclone activity: climatological features, linkages with the NAO and relationships with recent changes elsewhere in the Northern Hemisphere circulation. J. Climate 10, 453–464.

Serreze, M.C., Lynch, A.H., Clark, M.P., 2001. The Arctic frontal zone as seen in the NCEP-NCAR reanalysis. J. Climate 14, 1550–1567.

Serreze, M.C., Bromwich, D.H., Clark, M.P., Etringer, A.J., Zhang, T., Lammers, R., 2003. The large-scale hydro-climatology of the terrestrial Arctic drainage system. J. Geophys. Res. 108 (D2), 8160, doi:10.1029/2001JD000919.

Shinoda, M., 2001. Climate memory of snow mass as soil moisture over central Eurasia. J. Geophys. Res. 106 (D24), 33,393–33,403.

Sinclair, M.R., 1994. An objective cyclone climatology for the Southern Hemisphere. Mon. Weather Rev. 122, 2239–2256.

Sinclair, M.R., 1995. A climatology of cyclogenesis for the Southern Hemisphere. Mon. Weather Rev. 123, 1601–1619.

Wang, G.L., You, L.Z., 2004. Delayed impact of the North Atlantic Oscillation on biosphere productivity in Asia. Geophys. Res. Lett. 31, L12210, doi:10.1029/2004GL019766.

Yasunari, T., Kitoh, A., Tokioka, T., 1991. Local and remote responses to excessive snow mass over Eurasia appearing in the northern spring and summer climate: a study with the MRI GCM. J. Meteorol. Soc. Jpn. 69, 473–487.

Yu, R.C., Zhou, T.J., 2004. Impacts of winter-NAO on March cooling trends over subtropical Eurasia continent in the recent half century. Geophys. Res. Lett. 31, L12204, doi:10.1029/2004GL019814.